Structures 84 (2026) 111069

Contents lists available at ScienceDirect

Structures

journal homepage: www.elsevier.com/locate/structures

Seismic reliability assessment of base-isolated steel structures via Autoregressive Neural Network and Pearson distribution method

John Thedy [a,c], Iswandi Imran [b], Ay Lie Han [c,*], Marc Ottelé [d], Bobby Rio Indriyantho [c], Mochammad Qomaruddin [e]

[a] Formerly Department of Bioenvironmental Systems Engineering, National Taiwan University, Taipei, 106319, Taiwan
[b] Faculty of Civil and Environmental Engineering, Institut Teknologi Bandung, Bandung, 40132, Indonesia
[c] Department of Civil Engineering, Faculty of Engineering, Universitas Diponegoro, Semarang, 50275, Indonesia
[d] Microlab, Faculty of Civil Engineering and Geosciences, Delft University of Technology, Delft 2628 CN, the Netherlands
[e] Department of Civil Engineering, Faculty of Science and Technology, University Islamic of Nahdlatul Ulama, Jepara, 59427, Indonesia

ARTICLE INFO

Keywords:
Artificial Intelligence
Nonlinear Time History Analysis
Base isolation structure
Reliability analysis
Four-moment Pearson distribution

ABSTRACT

In seismic structural engineering, different methods are used to evaluate performance. Simplified approaches provide conservative estimates, while advanced analyses achieve higher precision at the cost of significant computational effort. Nonlinear Time History Analysis (NTHA) remains the most reliable method, but its high computational demand has led many researchers to propose simplified models, often resulting in conservative outcomes. This study proposes an Artificial Intelligence (AI)-based method to approximate NTHA. An Autoregressive Neural Network (ARNN) is developed to generate complete time-history responses of structures with minimal error relative to NTHA. Using ground motion data and the first three fundamental periods as inputs, the ARNN replicates NTHA responses with high accuracy. Unlike conventional surrogate models that predict only peak responses, the ARNN produces the entire response history. The ARNN is further integrated with a moment-based reliability framework employing the four-moment Pearson distribution (4M-Pearson), enabling efficient and accurate seismic reliability assessment. A three-story base-isolated steel structure is analyzed as a case study. Results demonstrate that the proposed ARNN achieves high precision in predicting both structural time-history responses and seismic reliability.

1. Introduction

In structural engineering, the primary objective is to ensure that a designed structure satisfies prescribed performance thresholds while accounting for inherent uncertainties in loads and material properties. To address these uncertainties, structural design often adopts a probabilistic framework. Unlike conventional approaches that apply safety factors without a clear link to safety levels, the probabilistic approach introduces load and capacity factors that explicitly define the structural reliability level [1,2]. From a probabilistic perspective, the probability of failure (P_f) of a structural system can be expressed as shown in Eq. (1).

$$P_f = \int_{G(\boldsymbol{\theta})\le 0} f_{\boldsymbol{\theta}}(\boldsymbol{\theta})d\boldsymbol{\theta} \tag{1}$$

The parameter set $\boldsymbol{\theta}$ represents the random variables associated with uncertainties in the system components, consisting of n_{rv} variables, i.e., $\boldsymbol{\theta} = \{\theta_1, \theta_2 \ldots, \theta n_{rv}\}$. A limit state function $G(\boldsymbol{\theta})$ is used to distinguish between safe and failed conditions, where failure occurs when $G(\boldsymbol{\theta}) < 0$. The function $G(\boldsymbol{\theta})$ may be defined in terms of drift or stress ratios, which commonly govern structural failure, while $\boldsymbol{\theta}$ may represent load and material parameters. The term $f(\boldsymbol{\theta})$ denotes the joint probability density function (PDF) of the system, often the PDF distribution of $G(\boldsymbol{\theta})$. Integrating $f(\boldsymbol{\theta})$ over the failure domain ($G(\boldsymbol{\theta}) < 0$) yields the probability of structural failure. Although mathematically feasible, defining the failure limit state is often complex and cannot always be expressed in closed-form equations, but rather through a series of simulations. For this reason, Eq. (1) is commonly reformulated into a discrete form, as shown in Eq. (2). Here, n_{sample} denotes the number of discrete samples, and $I[\cdot]$ is the failure indicator, which equals one if failure occurs and zero otherwise. In this approach, P_f is evaluated discretely through numerous simulation samples, a process referred to as Monte Carlo Simulation (MCS) [3] where it is known for its robustness but computationally

* Corresponding author.
E-mail address: hanaylie@live.undip.ac.id (A.L. Han).

https://doi.org/10.1016/j.istruc.2026.111069
Received 25 September 2025; Received in revised form 1 December 2025; Accepted 4 January 2026
Available online 8 January 2026

intensive.

$$P_{f(MCS)} = \frac{1}{n_{sample}} \sum_{i=1}^{n_{sample}} \{I[G(\boldsymbol{\theta}) \leq 0]\} \quad (2)$$

In seismic structural engineering, reliability assessment remains particularly challenging because the P_f is typically very low, requiring an extremely large number of MCS samples. Moreover, each seismic simulation is itself computationally demanding. These two factors make seismic reliability analysis especially resource-intensive. To address these challenges, researchers have proposed various frameworks, either by improving reliability assessment methods or by developing simplified yet conservative seismic design approaches.

From the reliability perspective, efforts to reduce the required sample size can generally be classified into three categories: sampling-based methods [4–10], response surface methods [11–17], and analytical methods [18–21]. Sampling-based methods retain the MCS framework but employ strategies to decrease the required number of samples. For example, Thedy et al. [6] proposed a multi-sphere importance sampling framework in which several hyperspheres are deployed within the safety domain to exclude unnecessary MCS samples, thereby reducing the number of function evaluations. Similarly, Au et al. [7] introduced subset simulation, which leverages conditional probability formulations to estimate extremely small failure probabilities through a sequence of more moderate failure probability events. In general, sampling-based methods manipulate either the geometry of the sampling domain or the sampling strategy itself to reduce computational demand. In contrast, response surface methods focus on replacing the original limit state function with an efficient surrogate model, thereby reducing the need for repeated evaluations of the true function. With the growing adoption and advancement of Artificial Intelligence (AI), such surrogates have gained increasing popularity. For instance, Echard et al. [14] applied the Kriging model to replicate complex limit state functions. The Kriging surrogate is constructed using a relatively small sample size, selected through adaptive sampling strategies to ensure both efficiency in sample number and effectiveness in capturing influential regions of the response surface. Unlike sampling-based or surrogate approaches, analytical methods aim to approximate the system PDF $f(\boldsymbol{\theta})$, as expressed in Eq. (1). Once $f(\boldsymbol{\theta})$ is formulated, the structural failure probability P_f can be evaluated through mathematical integration. The First-Order Reliability Method (FORM) [18] is one of the most widely adopted approaches due to its computational simplicity, where the limit state function is approximated using a linear Taylor expansion. More recently, Zhao et al. [20] introduced a surrogate PDF approach in which the distribution is constructed from the first three or four statistical moments, providing an efficient means to approximate the system reliability.

As mentioned earlier, beyond reliability methods, a major challenge in seismic reliability analysis lies in the seismic evaluation method itself. Design codes typically provide several options for evaluating structural performance. For example, the American Society of Civil Engineers (ASCE) code [22] permits four methods: Equivalent Lateral Force (ELF), Response Spectrum Method (RSM), Linear Time History Analysis (LTHA), and Nonlinear Time History Analysis (NTHA). Each method involves trade-offs between computational efficiency and result accuracy. Among these, ELF and RSM are the most computationally efficient, relying on critical assumptions to produce conservative designs with minimal computational effort. Both ELF and RSM analyze structures in the linear-elastic domain but introduce coefficients such as R (response modification factor) and C_d (deflection amplification factor) to approximate inelastic behavior. By contrast, NTHA provides the highest level of accuracy, as it captures both pre-peak and post-yield behavior of materials and structures. However, due to its step-by-step integration scheme and nonlinear treatment of stiffness and damping, NTHA requires substantial computational resources, making it impractical for routine design evaluations despite its accuracy.

This study aims to perform an efficient seismic reliability assessment of structures while preserving the accuracy of NTHA. Directly incorporating NTHA into reliability analysis remains computationally expensive compared to linear approach. Therefore, this work seeks to develop an alternative approach that achieves NTHA-level accuracy with substantially reduced computational effort. Several previous studies have investigated the seismic reliability assessment of structures [23–27]. Shen et al. [26], for example, employed the Probability Density Evolution Method (PDEM), which solves the Generalized Density Evolution Equation (GDEE) to construct the system PDF. Other studies [23,27] adopted Incremental Dynamic Analysis (IDA) to examine the effects of ground motion characteristics and variations in peak ground acceleration (PGA), and subsequently integrated reliability methods, such as moment-based approaches, to construct the system PDF. With advancements in computational power and AI, this study introduces an Autoregressive Neural Network (ARNN) model designed to generate complete time-history responses of structures. The ARNN takes as input the first three fundamental periods of the structure, along with previous ground motion and structural response data, to predict the next response step. Its autoregressive design enables the predicted response at each step to serve as input for the subsequent step, thereby producing a full time-history response. Training data for the ARNN are generated through extensive numerical simulations in SAP2000, covering various combinations of mass, stiffness, and ground motions. Since this work requires a large number of ground motion records, artificial seismic inputs are produced using the Kanai–Tajimi model [28]. Efforts to replace computationally intensive seismic evaluations have been reported in the literature [29–32]. However, most existing surrogate models predict only peak responses, such as maximum story drift or base shear. For example, Kim et al. [31] combined neural networks (NN) and convolutional neural networks (CNN) to predict maximum responses of single-degree-of-freedom systems. Other studies utilized machine learning to predict damage detection [33,34] or even serviceability level [35]. While such approaches achieve reasonable accuracy, they cannot fully replace NTHA, which provides complete time-history responses and more accurate result. For reliability analysis, this study adopts moment based reliability method from Zhao et al. [20]. Although the surrogate ARNN model is capable of efficiently predicting structural time-history responses, its autoregressive nature requires a large number of sequential predictions for each seismic simulation. As a result, adopting MCS with the ARNN still demands considerable computational effort. To address this, the present study integrates the ARNN with a moment-based method, specifically the four-moment Pearson distribution (4M-P), to construct the overall system failure PDF. This approach minimizes the required number of ARNN simulations while maintaining high accuracy in reliability estimation.

The paper is organized as follows. Section 2 highlights the novelty and significance of the proposed framework. Section 3 presents the methodology, including data collection and ARNN training procedures. Section 4 demonstrates the capability of the developed ARNN to predict structural time-history responses using a numerical example of a three-story structure equipped with a Bouc–Wen base isolation system, along with the corresponding reliability analysis using the 4M-P method. Section 5 provides concluding remarks, and Section 6 discusses the limitations and potential future research directions.

2. Research significance

Integrating seismic structural reliability analysis with NTHA remains computationally challenging. As discussed earlier, most previous studies have sacrificed accuracy to achieve feasible computation times, often relying on simplified seismic evaluation methods. In contrast, the present study develops an ARNN model capable of reproducing NTHA results with high accuracy while significantly reducing computation time. By further integrating this model with the 4M-P reliability assessment method, the proposed framework makes it possible to achieve seismic

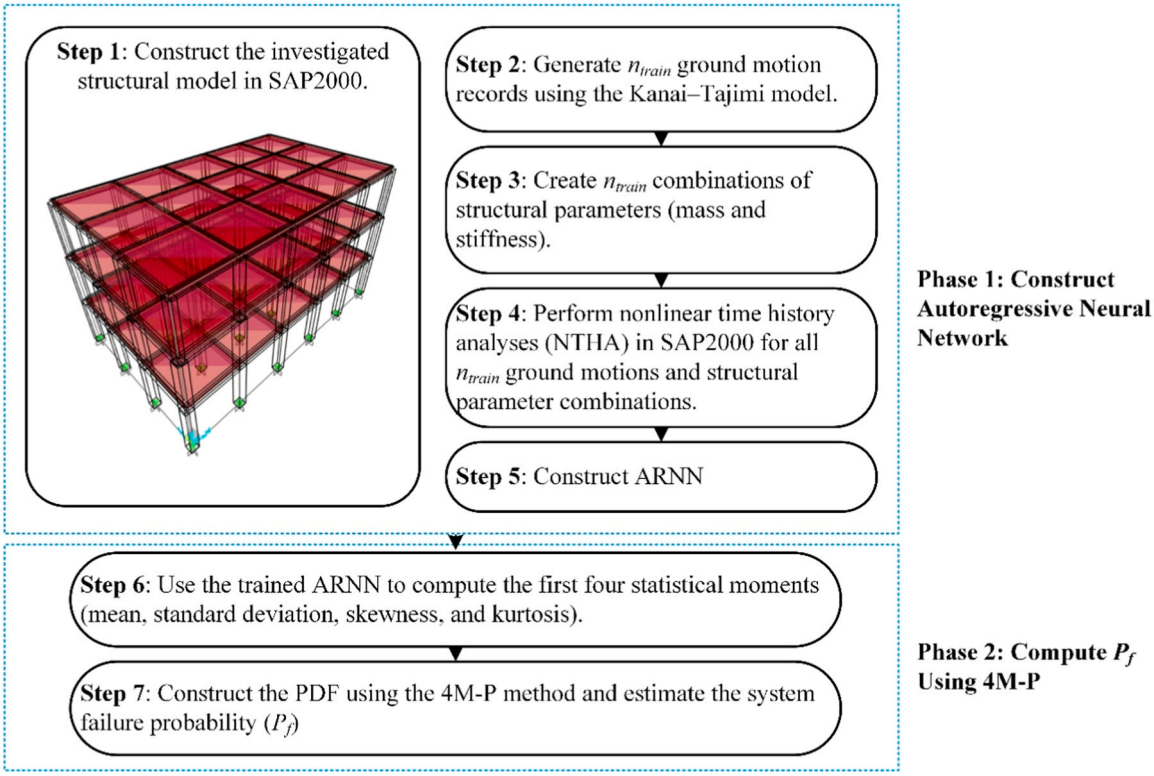

Fig. 1. General procedure of ARGNN construction.

reliability analysis with NTHA-level accuracy an outcome that was previously considered computationally challenging.

The key contributions and novel features of this study are summarized as follows:

1. The present study develops a simplified yet accurate ARNN model. While several studies have introduced AI-based models to replicate NTHA results [36–38], this work proposes a distinct ARNN framework that requires substantially fewer training samples. The model uses input features consisting of ground motions with varying characteristics and PGA, while structural properties are represented by fundamental periods rather than mass, stiffness, and damping parameters. This formulation yields a simpler yet highly accurate surrogate model. For the three-story base-isolated structure analyzed, only 100–150 SAP2000 simulations were needed to train the ARNN to a high level of accuracy. Section 4 presents a detailed comparison demonstrating the predictive performance of the proposed ARNN relative to SAP2000 results.
2. Integration of ARNN with a 4M-P for efficient reliability assessment. Direct application of MCS using the ARNN remains computationally demanding due to both the low probability of failure and the autoregressive nature of the model. To overcome this, the study adopts the 4M-P method, which requires only 50–100 ARNN predictions to compute the first four statistical moments that serve as inputs for the Pearson distribution. Since the ARNN is designed to accommodate variations in structural properties and ground motions, the resulting reliability assessment inherently accounts for uncertainties in both loading and structural parameters.
3. The constructed ARNN is trained to predict the structural response time history based on ground motion and structural parameters. When integrated with the 4M-P method for reliability assessment, the framework can incorporate both record-to-record variability of seismic ground motions and uncertainties in structural parameters. This combination enables seismic structural reliability analysis with NTHA-level accuracy an achievement rarely reported in the literature.

3. Methodology

This study primary objective is to assess reliability of structure considering uncertainty from ground motion record to record variability and structure parameter uncertainty sourced from mass and stiffness. To attain this objective, the framework general scheme procedure is presented in Fig. 1. The overall procedure consists of two major phases in which Phase 1: Construct Autoregressive Neural Network model the followed with Phase 2: Compute P_f using 4M-P method. The first phase has objective to construct accurate ARNN model that produce complete structure response time history. The detail description on Phase 1 and 2 will be explained in Sections 3.1 and 3.2 respectively.

3.1. Construct Autoregressive Neural Network (ARNN)

This phase requires the collection of training data through ground motion generation and structural simulations with varying parameters, paired systematically to cover a wide range of scenarios. To automate the NTHA, the SAP2000 Open Application Programming Interface (OAPI) is employed, enabling large-scale simulations. The overall ARNN construction process is summarized in the following steps:

- **Step 1**: The structural model is developed in SAP2000 to perform NTHA. A script-based modeling approach is adopted through the SAP2000 OAPI, enabling automated generation of multiple simulation cases. In this step, the upper and lower bounds of structural parameters and ground motion properties are also defined, along with the number of training samples n_{train}. Typically, 100–300 simulations are sufficient to train the model for structures ranging from three to six stories.
- **Step 2**: A total of n_{train} ground motions are generated using the Kanai–Tajimi model. This study does not impose restrictions on the

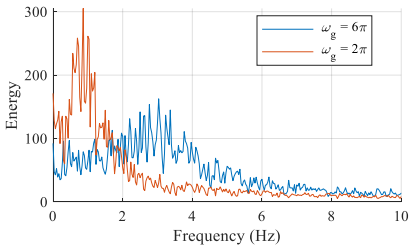

(a) Response Spectrum of Random Generated Motions Assuming Normal Distribution Parameter with COV=0.1 and Mean Value ω_g=π ,ξ_g=0.3 ,σ_g=0.3 ,T_{90}=0.3 ,*eps*=0.3.

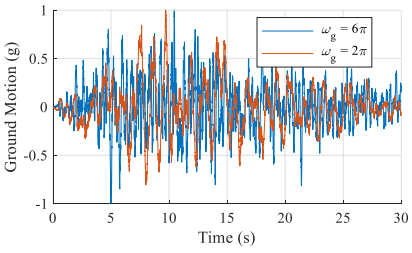

(b) Generated Ground Motions Using Dominant Period of 2s and 0.5s.

Fig. 2. Random generated artificial ground motions response spectrum.

type of ground motion generation technique used; when sufficient real earthquake records are available, their use is generally preferable. However, the selected approach must allow flexible adjustment of ground-motion parameters during the reliability analysis phase. A ground-motion database is not employed in this study due to the limited availability of records exhibiting the specific frequency characteristics required for ARNN training and parameter variability. Consequently, the present work adopts the Kanai–Tajimi artificial ground-motion generator [28] without any modification to produce the seismic inputs for both ARNN training and reliability assessments. The Kanai–Tajimi model implementation used in this study is based on an open-source MATLAB code provided in the referenced literature [39]. The original Kanai–Tajimi model defines a power spectral density function (S) to characterize earthquake motions based on a single-degree-of-freedom (SDOF) assumption, as expressed in Eq. (3).

$$S = S_0 \frac{\omega_g^4 + \left(2\xi_g\omega_g\omega\right)^2}{\left(\omega_g^2 - \omega^2\right) + \left(2\xi_g\omega_g\omega\right)^2} \tag{3}$$

$$S_0 = \frac{2\xi_g\sigma_g^2}{\pi\omega_g\left(4\xi_g^2 + 1\right)} \tag{4}$$

Where ω_g and ξ_g are ground frequency and damping ratio, S_0 defined as constant spectral intensity on bed rock. While ω is the frequency vector for power spectral density construction. S_0 could be defined using Eq. (4) where σ_g^2 defines the ground acceleration variance. The Kanai–Tajimi model is commonly utilized because it can reproduce ground motion characteristics through controllable parameters such as dominant frequency and variance. Nevertheless, accelerations generated directly from Eq. (3) correspond to a stationary process, while actual earthquake records are inherently non-stationary. To overcome this discrepancy, an envelope function is introduced, modifying the stationary Kanai–Tajimi excitation into a time-dependent form. The mathematical expression of this envelope function is given in Eq. (5).

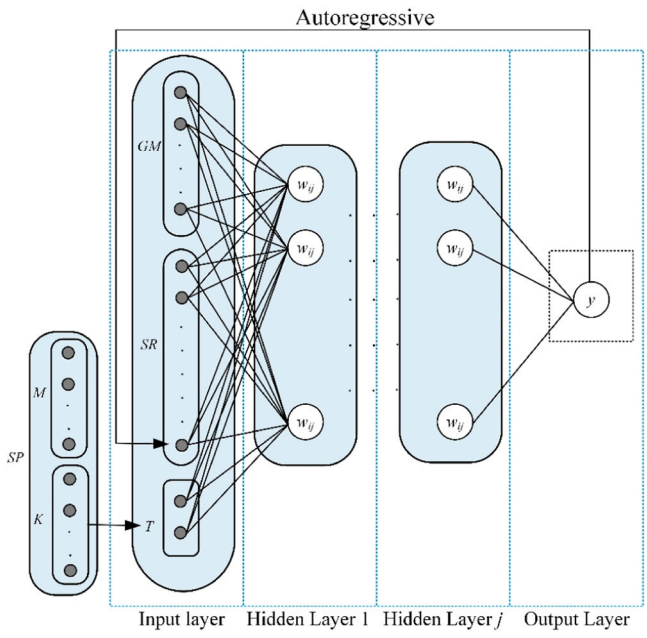

Fig. 3. Network architecture of ARNN.

$$E(t) = \left(\frac{e}{eps}\frac{t}{t_n}\right)^{-\frac{eps(\log(T_{90}))}{1+eps(\log(T_{90})-1)}} \exp\left(\frac{eps(\log(T_{90}))}{1+eps(\log(T_{90})-1)}\frac{t}{eps\times t_n}\right) \tag{5}$$

Where *eps*, t_n, and T_{90} defined as normalized duration at peak, ground motion duration, and value at 90 % of the duration. The envelope function adjusts only the amplitude of the motion, shaping the acceleration history to resemble seismic activity while maintaining the original ground motion characteristics described in Eq. (3) and Eq. (4). To generate ground motions, five key parameters in which ω_g, ξ_g, σ_g, T_{90}, and *eps* from Eqs. (3)–(5) are taken as random generated number follow normal distribution with COV (Coefficient of Variation) = 0.1. Fig. 2 illustrates the response spectrum of the randomly generated ground motions. In Fig. 2(a), the response spectrum for a dominant period of 0.5 s is shown, demonstrating that the algorithm successfully generates acceleration spectra with the intended dominant frequency and spectral shape. Meanwhile, Fig. 2(b) presents a comparison of ground motions generated for dominant periods of 2.0 s and 0.5 s using the Kanai-Tajimi algorithm.

- **Step 3**: Generate n number of mass and stiffness of structure combination. This combination later will be paired with n ground motion for NTHA analysis to generate training data. As shown in Step 2 and 3, training data has variation in ground motion record to record variability and structure parameter, that makes the constructed ARNN later could handle various input of ground motion and structure parameter. Further, the computer reliability analysis at later step could accounted the uncertainty in ground motion and structure parameters and high accuracy of NTHA result.

- **Step 4**: Perform NTHA analysis using SAP2000. This step is performed automatically using OAPI feature from SAP2000. The n_{train} number of ground motion and structure parameters is assigned into structure constructed in Step 1 to generate n_{train} number of structure response. The response on each floor of structure together with input ground motion, structure parameters and structure periods are recorded for training data.

- **Step 5**: Once the training data are generated in Step 4, the next stage is the development of the ARNN. The detailed architecture of the

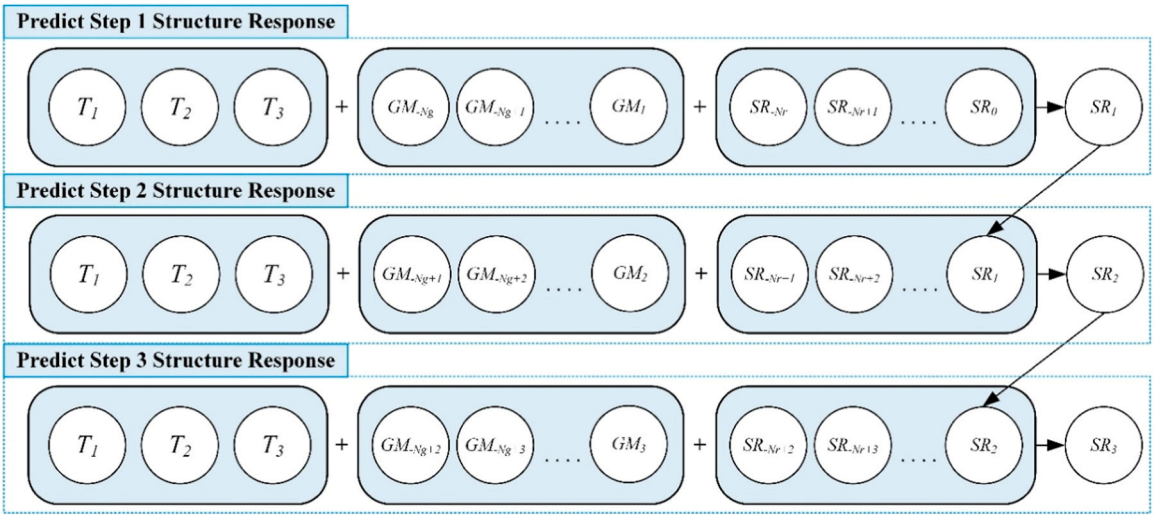

Fig. 4. Autoregressive scheme of ARNN.

proposed ARNN is illustrated in Fig. 3. The ARNN is designed in an autoregressive manner, meaning that the predicted output at step i is used as part of the input for step $i+1$. By repeating this process throughout the entire ground motion duration, a complete structural response time history can be obtained. Fig. 4 further illustrates the autoregressive prediction mechanism. The ARNN incorporates three input segments, as shown in Fig. 3 and Fig. 4. First, Structural Properties (*SP*) are represented not by mass, stiffness, and damping directly, but by the first two fundamental periods (T) extracted through modal analysis. This approach provides a compact yet effective representation of structural characteristics.

Second, Ground Motion (*GM*) input is included by taking several preceding steps of the acceleration record. Specifically, to compute the structural response at time step 1, the ground motion data from steps $1-N_{wg}$ to 1 are used, where N_{wg} denotes the number of preceding ground motion steps. In this study, $N_{wg} = 25$. Third, the previous Structural Response (*SR*) history is also provided as input. Unlike the ground motion input, which includes data up to the current step, the structural response input spans from steps $1 - N_{wr}$ to 0, i.e., the step immediately prior to the target response step. The optimal values of N_{wg} and N_{wr} were determined through a trial-and-error process. For N_{wr}, the recommended value is equal to at least cover the half of the first fundamental period time window. For example, if the fundamental period of structure is 1.5 s and the time increment of NTHA is 0.005 s, then half of fundamental period is 0.75 s divided by 0.005 s, which is equivalent to $N_{wr} = 150$. Assigning larger value of N_{wr} will be conservative but required more computation time while not sufficient N_{wr} value results in lower prediction accuracy. For both the NTHA and ARNN analyses, a fixed time increment of 0.005 s is employed to ensure consistency between the numerical simulations and the autoregressive predictions.

3.2. Failure probability (P_f) assessment using 4M-P

After constructing the ARNN, the framework proceeds to the second phase, where reliability assessment is conducted to evaluate P_f. Surrogate models such as response surface method are commonly paired with MCS, as their predictions require negligible computational cost. However, due to the autoregressive nature of ARNN, thousands of predictions are still required for a single ground motion record. When very small failure probabilities are considered, combining ARNN with MCS remains computationally demanding. To address this issue, the present study integrates ARNN with an analytical reliability method, namely the 4M-P approach. Compared with sampling-based approaches, analytical methods require fewer samples but may exhibit reduced accuracy for highly nonlinear problems, particularly in the case of FORM, which relies only on the first two statistical moments. In contrast, the 4M-P method incorporates up to the fourth moment, providing improved representation of nonlinear failure limit states. This phase, employing the 4M-P method, consists of two main steps, as described below.

- **Step 1**: The first four moments of the failure limit state are computed using the ARNN predictions. These moments are defined as shown in Eq. (6), where the time history ARNN output transformed into structure failure indicator ($\widehat{G}$) to represents the structural condition. In this study, the first four moments are denoted as α_1 (mean), α_2 (standard deviation), α_3 (skewness), and α_4 (kurtosis). While Zhao et al. [20] employed the point estimation method to calculate moments, the present study evaluates each sample using the ARNN, enabling a more robust computation as expressed in Eq. (6). In Section 4, the effect of different sample sizes (n_{sample}) on the accuracy of the computed moments will be compared against MCS results.

$$\begin{aligned}
\alpha_1 &= \frac{1}{n_{sample}} \sum_{i=1}^{n_{sample}} \widehat{G}_i \\
\alpha_2 &= \sqrt{\frac{1}{n_{sample}} \sum_{i=1}^{n_{sample}} (\widehat{G}_i - \alpha_1)^2} \\
\alpha_3 &= \frac{\frac{1}{n_{sample}} \sum_{i=1}^{n_{sample}} (\widehat{G}_i - \alpha_1)^3}{\alpha_2^3} \\
\alpha_4 &= \frac{\frac{1}{n_{sample}} \sum_{i=1}^{n_{sample}} (\widehat{G}_i - \alpha_1)^4}{\alpha_2^4}
\end{aligned} \tag{6}$$

- **Step 2**: In the second step, once the system moments have been determined, the Pearson distribution PDF is constructed using the formulation shown in Eq. (7). Unlike conventional distributions that rely only on the first two moments (mean and standard deviation), the Pearson distribution incorporates information from the first four moments. Evaluating these moments, as described in the previous step, requires far fewer samples than directly estimating P_f, particularly for systems with extremely low failure probabilities. As indicated in Eq. (7), the Pearson distribution consists of multiple types, from TYPE 0 to TYPE 7, with the specific type determined by the computed variables a, b, c, d, r_0, r_1, r_2, and Δ. These equations are

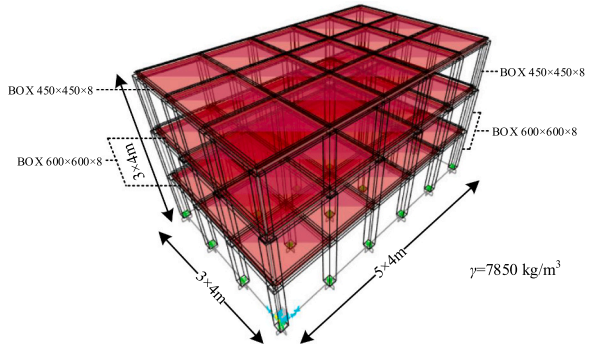

Fig. 5. Three story structure with base isolation.

calculated based on α_3 (skewness) and α_4 (kurtosis). The resulting PDF initially has zero mean and unit standard deviation; it is then adjusted using the identified α_1 and α_2. Using this adjusted PDF, the failure probability P_f is computed according to the concept in Eq. (1). By applying this approach with the surrogate PDF from Eq. (7), the final P_f is obtained as formulated in Eq. (8). Where $\boldsymbol{x}$ is a set of random variables vector in standard normal dimension.

$$\text{TYPE0}: f(x) = \frac{1}{\sqrt{2\pi}}\exp\left(\frac{-x^2}{2}\right) \rightarrow \Delta = 0 \cap b = 0$$

$$\text{TYPE1}: f(x) = (x - r_2)^{\frac{-ar_2 - b}{\sqrt{\Delta}}}(r_2 - x)^{\frac{ar_1 + b}{\sqrt{\Delta}}} \rightarrow \Delta > 0 \cap b \neq 0 \cap d < 0$$

$$\text{TYPE2}: f(x) = \left(-\frac{c}{d} - x^2\right)^{-\frac{a}{2d}} \rightarrow \Delta > 0 \cap b = 0$$

$$\text{TYPE3}: f(x) = (c + bx)^{\frac{ac - b^2}{b^2}\exp\left(-\frac{az}{b}\right)} \rightarrow \Delta > 0 \cap b \neq 0 \cap d = 0$$

$$\text{TYPE4}: f(x) = \left(c + bx + dx^2\right)^{-\frac{a}{2d}}\exp\left(\left(\frac{ab - 2bd}{d\sqrt{-\Delta}}\right)\tan^{-1}\left(\frac{b + 2dx}{\sqrt{-\Delta}}\right)\right) \rightarrow \Delta < 0 \cap b \neq 0$$

$$\text{TYPE5}: f(x) = |x - r_0|^{-\frac{a}{d}}\exp\left(\frac{ar_0 + b}{d(x - r_0)}\right) \rightarrow \Delta = 0 \cap b \neq 0$$

$$\text{TYPE6} - 1: f(x) = (r_1 - x)^{\frac{ar_1 + b}{\sqrt{\Delta}}}(r_2 - x)^{\frac{ar_1 + b}{\sqrt{\Delta}}} \rightarrow \Delta > 0 \cap b < 0 \cap d > 0$$

$$\text{TYPE6} - 2: f(x) = (x - r_1)^{\frac{ar_1 + b}{\sqrt{\Delta}}}(x - r_2)^{\frac{ar_1 + b}{\sqrt{\Delta}}} \rightarrow \Delta > 0 \cap b > 0 \cap d > 0$$

$$\text{TYPE7}: f(x) = \left(\frac{c}{d} + x^2\right)^{-\frac{a}{2d}} \rightarrow \Delta < 0 \cap b = 0$$

$$a = 10\alpha_4 - 12{\alpha_3}^2 - 18 \quad c = 4\alpha_4 - 3{\alpha_3}^2 \quad \Delta = b^2 - 4cd \quad r_1 = \frac{-b - \sqrt{\Delta}}{2d}$$
$$b = \alpha_3(\alpha_4 + 3) \quad d = 4\alpha_4 - 3{\alpha_3}^2 \quad r_0 = -\frac{b}{2d} \quad r_2 = \frac{-b - \sqrt{\Delta}}{2d} \tag{7}$$

$$P_f = \int_{G \leq 0} f_{\boldsymbol{x}}(\boldsymbol{x}\alpha_2 + \alpha_1) \tag{8}$$

4. Numerical example: three-story steel structure equipped with base isolation

This section presents a numerical example using a three-story steel structure equipped with base isolation. Fig. 5 illustrates the structural geometry and section details. Several design codes permit the use of a linearized base isolation model, in which the isolator is represented by an equivalent linear spring and damping value derived from its mechanical properties, as demonstrated in previous studies [40–42]. This linearization enables the use of LTHA, offering significant computational savings at the cost of reduced accuracy due to the simplification of nonlinear isolator behavior. In contrast, the present study aims to employ an AI-based approach that closely replicates the NTHA response with minimal error.

In the current numerical example, the structure is assumed to be constructed with A36 steel. The base isolation is modeled using a Bouc–Wen spring element, with an elastic stiffness $K = 4.5$ kN/mm and effective stiffness $K_{eff} = 1.1$ kN/mm. The isolator is assumed to have a yield force of 57 kN and a post-yield stiffness ratio of 0.2. Typically, structures with base isolation are designed to remain elastic under design-level earthquakes; therefore, in this numerical example, the structure is assumed to remain elastic, with nonlinearity arising solely from the base isolation device. Rayleigh proportional damping of 3 % is applied to two selected periods, 0.01 s and 5 s, to account for higher-mode and nonlinear-period responses, respectively. NTHA is performed using the commercial software SAP2000, employing the Hilber–Hughes–Taylor (HHT) direct integration method, with $\alpha = 0.5$ and $\beta = 0.25$. The NTHA results from SAP2000 are used both for training the ARNN and for validation.

The presented structure is intended solely to demonstrate the ARNN prediction accuracy and the reliability evaluation framework described in Section 3; therefore, the geometry in Fig. 5 does not fully comply with any design code. The focus of this example is on assessing the accuracy of the ARNN relative to SAP2000 NTHA results and evaluating the efficiency of the P_f computation using a limited number of samples. This section is divided into two subsections. Section 4.1 presents the ARNN construction, including the training data generation process, boundary conditions, and ARNN hyperparameters. The prediction accuracy of the ARNN-generated structural response time histories is compared to SAP2000 results. Section 4.2 demonstrates the computation of the failure probability (P_f) using the Pearson distribution-based 4M-P method.

Table 1
Considered ground motion parameters.

Ground Motion Training Data					
Random Variable	Symbol	Mean	Unit	COV	Distribution
Standard deviation of excitation	σ_g	0.3	-	0.1	Normal
Site damping ratio	ζ_g	0.3	%		
Value at 90 % of the duration	T_{90}	0.3	g		
Normalized duration time when peak occurred	*eps*	0.3	-		
Peak Ground Acceleration	*PGA*	0.2	g		
Dominant frequency of earthquake excitation	ω_n	2	rad	0.2	

4.1. Construction of ARNN and prediction accuracy

Using the method described in Section 3.1, the ARNN model is constructed to predict the displacement time history of each story. It should be noted that a separate ARNN model is developed for each story. The network architecture consists of four hidden layers, each with 50

Table 2
Lower and upper bound limit for structure parameters.

Random Variable	Symbol	Unit	Lower limit	Upper Limit
Live Load on Story 1, 2, 3	*LL*	tf/m^2	0.1	0.3
Elastic Modulus on Story 1, 2, 3	*E*	MPa	1×10^5	3×10^5

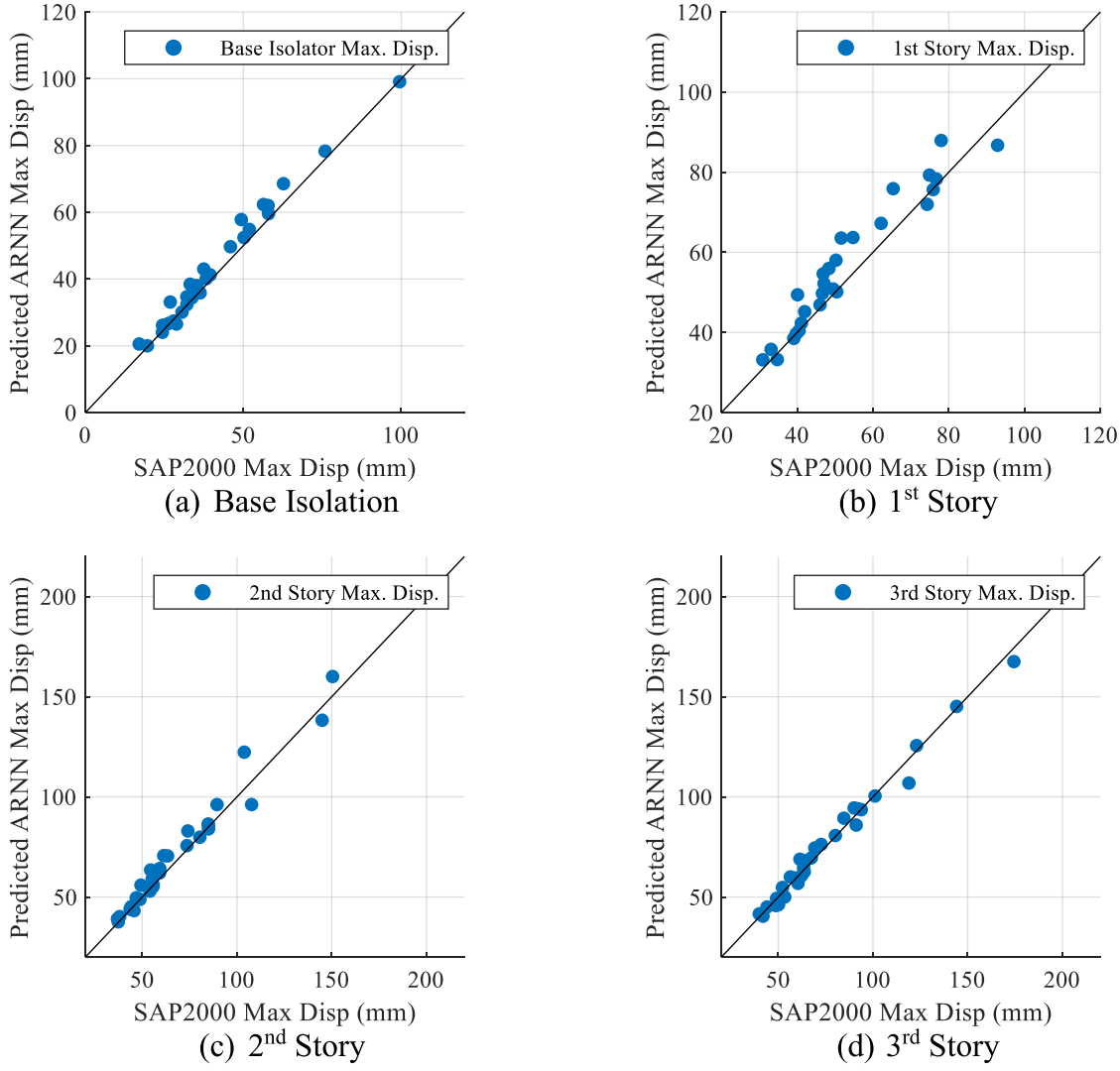

Fig. 6. Validation result on maximum displacement of ARNN prediction vs SAP2000 result.

nodes. The training is performed using a Limited-memory Broyden–-Fletcher–Goldfarb–Shanno (L-BFGS) quasi-Newton algorithm, which minimizes the mean squared error (MSE). The L-BFGS solver employs a standard line-search method with an approximation of the Hessian matrix. The training process is terminated after 1.5×10^4 iterations. The seismic time increment is set to 5×10^{-3} s. Table 1 and Table 2 present the boundaries of the variables considered for ground motion variability and structural components, respectively. Parameters σ_g, ζ_g, T_{90}, eps, t_n, and ω_n control the characteristics of the generated ground motions within the Kanai–Tajimi model, as described in Section 3.1. With the base isolation in place, the numerical structure exhibits a fundamental period of 1.45 s when the structural parameters are assigned their mean values. Dead load is assumed to be 0.2 tf/m^2, and the total structural mass is derived from self-weight, dead load, and half of the live load. These loads are applied prior to performing the NTHA.

In this numerical example, 125 samples of ground motion parameters, as listed in Table 1, are generated using a Latin Hypercube Sampling (LHS) strategy, assuming a normal distribution. These are paired with 125 samples of structural parameters, generated via LHS with uniform distributions within the boundaries specified in Table 2. The resulting 125 combinations of ground motion and structural parameters are used as training data for NTHA simulations. In addition to the NTHA response records, the first two modal periods obtained from modal analysis are included as input for the ARNN training, as described in Section 3.1.

Table 3
Measured error on 30 testing data.

Error Indicator on 30 Testing Data	Maximum Displacement			
	Base Isolation	1st Story	2nd Story	3rd Story
MAPE (%)	7.04	7.76	5.81	4.22
MAE (mm)	2.74	4.37	4.18	3.07
RMSE (mm)	3.48	5.58	6.01	3.96
R^2	0.99	0.99	0.98	0.99

After training the ARNN, an independent set of 30 ground motion and structural parameter samples is generated outside the training dataset for validation. These samples cover a range of ground motion characteristics, structural properties, and seismic intensities, with parameters randomly selected within the boundaries defined in Table 1 and Table 2. Each of these 30 cases is analyzed using NTHA in SAP2000, and the results are used to validate the ARNN predictions. Fig. 6 presents the maximum story displacement predicted by the ARNN against the corresponding SAP2000 results. Prediction accuracy is evaluated using four metrics: Mean Absolute Percentage Error (*MAPE*), Mean Absolute Error (*MAE*), Root Mean Square Error (*RMSE*), and the coefficient of determination (R^2). Table 3 summarizes these error metrics for each

Table 4
Several testing data for validation.

Test	Story						Artificial EQ parameter					
	Modulus ($\times 10^3$ MPa)			Live Load ($\times 10^{-1}$ tf/m^2)			PGA (g)	ζ	σ	f_{EQ}	T_{90}	*eps*
	1	2	3	1	2	3						
1	286.43	245.57	168.42	1.86	1.04	1.33	0.21	0.31	0.32	2.10	0.32	0.28
2	106.52	114.70	232.47	1.63	2.56	1.68	0.28	0.26	0.27	1.87	0.29	0.31
3	219.06	237.37	202.90	2.42	1.71	2.98	0.19	0.27	0.29	2.19	0.31	0.29

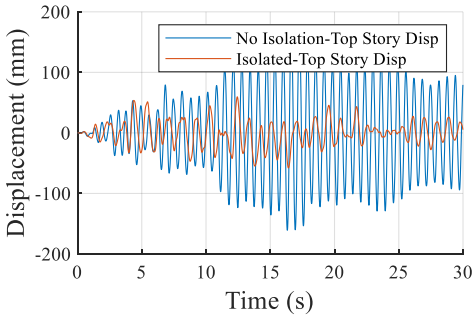

(a) Top-story displacement time histories for fixed-base (non-isolated) and base-isolated structures

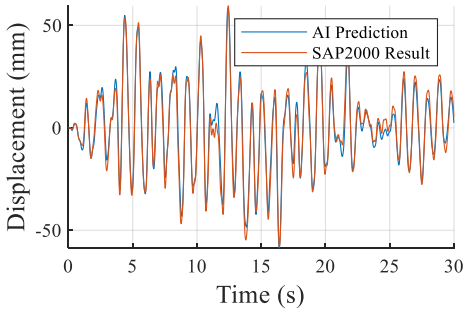

(b) Comparison of ARNN-predicted and SAP2000 top-story displacement histories

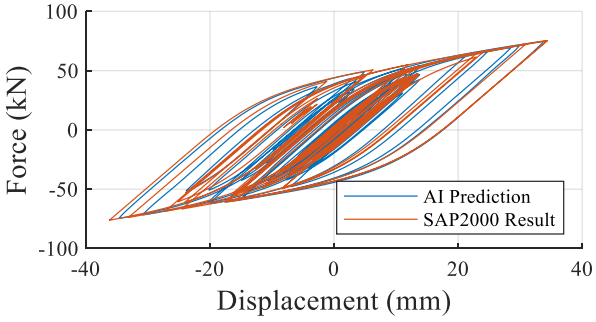

(c) Hysteresis curves of the base isolation from ARNN and SAP2000

Fig. 7. Result of test 1 (structure $T_{fund} = 1.41$ s).

story, including the base isolation. The ARNN demonstrates high accuracy, with *MAPE* ranging from 4.22 % to 7.76 %, R^2 values above 0.98, and relatively low *MAE* and *RMSE* values.

Since the ARNN produces the complete time history response, presenting all 30 test cases within this article is impractical. Therefore, only three representative cases are shown, with parameters listed in Table 4. These cases cover ground motions with varying characteristics and PGA ranging from 0.19 to 0.28 g, as well as structural parameters in terms of mass and stiffness. Figs. 7–9 presents the NTHA results and ARNN predictions for the cases in Table 4. It includes: (a) top-story displacement time histories for fixed-base (non-isolated) and base-isolated structures, (b) comparison of ARNN-predicted and SAP2000 top-story displacement histories, and (c) hysteresis curves of the base isolation from ARNN and SAP2000. The structural periods for these cases range from 1.41 s to 1.52 s. The comparison between fixed-base and base-isolated responses illustrates the significance of base isolation nonlinearity in the overall structural response. For the three test cases, the average reduction in top-story displacement due to base isolation is approximately 50 %, which is consistent with typical base isolation performance.

The ARNN predictions closely match the NTHA results, capturing both displacement time histories and base isolator hysteresis behavior. All computations were performed on an Intel 13th Gen i7-1360P CPU. While a single NTHA simulation requires approximately 20 min, the ARNN predicts the complete time history for a single ground motion in about 2 s, demonstrating a significant reduction in computational effort.

From Fig. 7–9, it is evident that the constructed ARNN accurately reproduces the displacement time histories obtained from SAP2000. Moreover, the ARNN effectively accounts for record-to-record variability in ground motion as well as variations in structural parameters, including story stiffness and mass.

4.2. Failure probability (P_f) assessment using 4M-P

With the surrogate model constructed in Section 4.2, reliability assessment is performed in this section using the 4M-P method. This moment-based approach computes the failure probability (P_f) by first

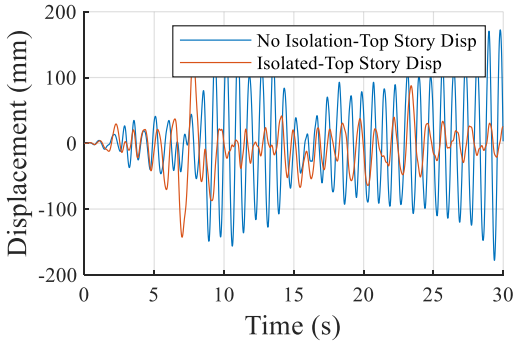

(a) Top-story displacement time histories for fixed-base (non-isolated) and base-isolated structures

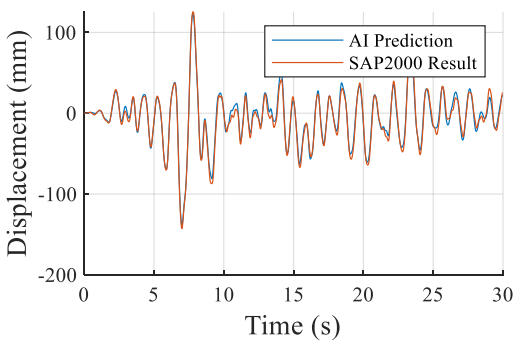

(b) Comparison of ARNN-predicted and SAP2000 top-story displacement histories

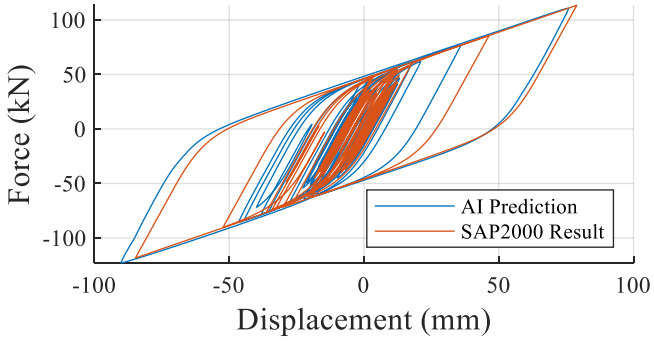

(c) Hysteresis curves of the base isolation from ARNN and SAP2000

Fig. 8. Result of test 2 (structure $T_{fund} = 1.52$ s).

determining the first four moments of the limit state function, which are then used to construct a Pearson distribution. The resulting surrogate PDF represents the probability distribution of the limit state function. Table 5 lists the assumed random variables for the investigated structure. In this study, uncertainties are considered to originate from *SP*, including mass and stiffness, and *GM* parameters, including Kanai–Tajimi parameters and PGA. Based on previous studies [43], the largest source of uncertainty arises from ground motion variability, including PGA. Consequently, the uncertainties associated with the base isolation parameters are assumed negligible and are not considered in this study. For the numerical example, failure is defined as the event where the story drift ratio exceeds a threshold δ. The failure probability is formulated as shown in Eq. (9)., where $f(\boldsymbol{x},\alpha_1,\alpha_2)$ is the Pearson PDF constructed using the four moments. Since the surrogate PDF is known, the failure probability can be computed using numerical integration over the failure domain. The drift ratio is obtained directly from the ARNN-predicted time history responses. As shown in Section 4.1, the ARNN provides highly accurate predictions, with maximum displacement errors in terms of MAPE ranging from 4 % to 7 %.

$$P_f = \int_{\hat{G}(SP,GM)\leq\delta} f_{\mathbf{x}}(\boldsymbol{x}\alpha_2 + \alpha_1)d\boldsymbol{x} \tag{9}$$

In this study, the first four moments of the system mean, standard deviation, skewness, and kurtosis are computed using different sample sizes to investigate their sensitivity. Table 6 presents the identified moments obtained with sample sizes of 400, 600, and 800 using Eq. (7). The computation procedure has been described in Section 3.2. Each sample set is evaluated using the ARNN, which provides a significantly more efficient approach compared to performing full NTHA. As shown in Table 6, the values of α_1 (mean) and α_2 (standard deviation) exhibit minimal variation across sample sizes of 400 and 600. However, for higher-order moments, α_3 (skewness) and α_4 (kurtosis), convergence is achieved only when the sample size approaches 800.

Using this computed moments of different sample size, Pearson distribution PDF is constructed as shown in Fig. 10(a)–(c) showing the PDF of top story, 2nd story, and 1st story respectively.

Besides the 4M-P PDF estimation, two additional methods MCS using ARNN (MCS + ARNN) and MCS integrated with the Equivalent Linearized Method (MCS + ELM) were also conducted for comparison. For the MCS + ARNN, a PDF was constructed using 3000 Monte Carlo samples, as shown in Fig. 10. It should be noted that this MCS was performed using the surrogate ARNN model to generate structural responses for each sample. The purpose of including the MCS + ARNN approach is to demonstrate the accuracy and efficiency of the 4M-P method, which can construct a comparable PDF using a much smaller sample size than the 3000 samples required by MCS + ARNN. Performing MCS directly with NTHA while accounting for ground-motion variability and structural parameter randomness is computationally prohibitive in this study. As discussed in Section 4.1, a single NTHA requires approximately 20 min, making large-scale MCS infeasible. Although the ARNN predictions significantly reduce computational cost, MCS with ARNN still remains challenging, as accurate reliability assessment typically requires hundreds of thousands of samples. Therefore, in the present study, the MCS + ARNN simulation is limited to 3000 samples due to computational constraints.

The third reliability assessment method evaluated in this study is MCS + ELM, in which the reliability analysis is performed through MCS while the structural responses are obtained using LTHA based on the Equivalent Linearized Method. This method is widely adopted and permitted in seismic design codes. In the present study, the ELM

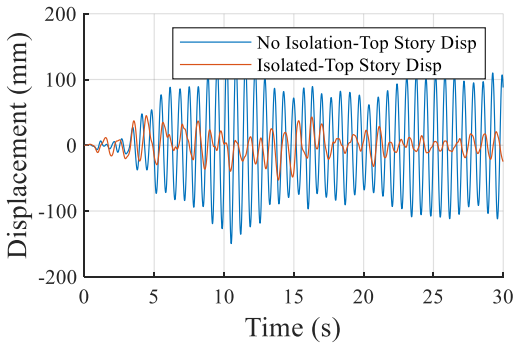

(a) Top-story displacement time histories for fixed-base (non-isolated) and base-isolated structures

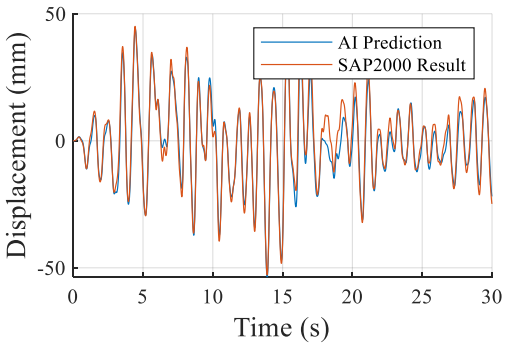

(b) Comparison of ARNN-predicted and SAP2000 top-story displacement histories

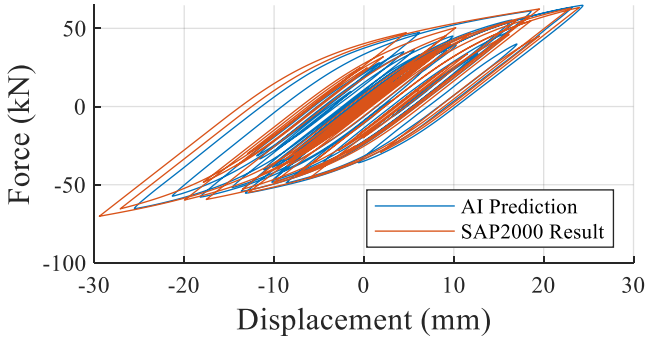

(c) Hysteresis curves of the base isolation from ARNN and SAP2000

Fig. 9. Result of test 3 (structure $T_{fund} = 1.45$ s).

Table 5
Considered random variables.

Random Variable	Symbol	Mean	Unit	COV	Distribution
Uncertainty Sourced from Ground Motion					
Standard deviation of excitation	σ_g	0.3	-	0.1	Normal
Site damping ratio	ζ_g	0.3	%		
Value at 90 % of the duration	T_{90}	0.3	g		
Normalized duration time when peak occurred	*eps*	0.3	-		
Peak Ground Acceleration	*PGA*	0.2	g		
Dominant frequency of earthquake excitation	ω_n	2	rad	0.2	
Uncertainty Sourced from Ground Motion					
Live Load on Story 1, 2, 3	*LL*	0.2	tf/ m^2	0.1	Normal
Elastic Modulus on Story 1, 2, 3	*E*	2×10^5	MPa		

procedure follows ASCE 7-22, where the base isolator is idealized as a linear spring characterized by an effective stiffness (K_{eff}) and effective damping (ζ_{eff}), computed using Eq. (10).

$$K_{eff} = \frac{|F^+| + |F^-|}{|\Delta^+| + |\Delta^-|}$$
$$\varsigma_{eff} = \frac{2}{\pi} \frac{E_{loop}}{K_{eff}(|\Delta^+| + |\Delta^-|)^2} \tag{10}$$

Here $|F^+|$and $|F^-|$ denote the peak positive and negative isolator forces, which are equal to 220 kN in this study. Similarly, $|\Delta^+|$and$|\Delta^-|$ represent the peak positive and negative isolator displacements, equal to 200 mm. E_{loop} is the energy dissipated within a single hysteresis cycle. Using Eq. (10), the computed values of K_{eff} and ζ_{eff} are 1.1kN/mm and 0.126, respectively. With these effective properties, the base isolator is modeled as a linear spring having stiffness K_{eff} and damping ratio ζ_{eff}. Subsequently, LTHA combined with MCS is used to construct the corresponding PDF, labeled as MCS + ELM in Fig. 10, using 3000 samples.

Table 6
Computed moments using different sample size.

Story Drift (δ)	n_{sample}	Moments			
		α_1 (Mean)	α_2 (Standard Deviation)	α_3 (Skewness)	α_4 (Kurtosis)
Top Story	400	0.31	0.10	1.33	5.71
	600	0.32	0.10	1.49	6.70
	800	0.31	0.09	1.47	6.80
2nd Story	400	0.30	0.10	3.02	26.05
	600	0.31	0.10	2.48	19.26
	800	0.31	0.09	2.26	17.20
1st Story	400	0.62	0.20	2.49	16.63
	600	0.62	0.19	2.21	14.55
	800	0.62	0.19	2.05	12.98

As shown in Fig. 10, the proposed 4M-P approach successfully reproduces the PDF generated by MCS. For a more detailed comparison, the failure probability (P_f) is evaluated under drift ratio thresholds of 0.5 %, 0.75 %, and 1.00 % using discrete integration. Table 7 summarizes the comparison of P_f values obtained from MCS and 4M-P, along with the error ε, defined as the difference between the two approaches. The results show that for $P_f > 0.2$, the relative error remains below 10 %.

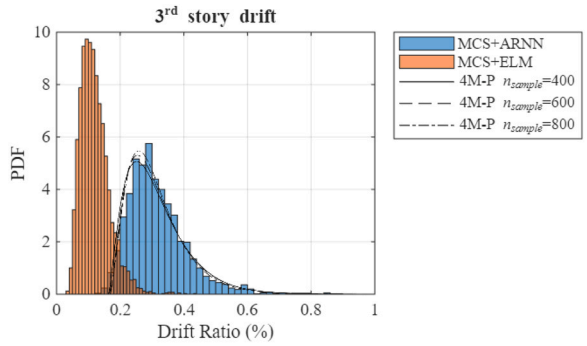

(a) Top Story Drift PDF.

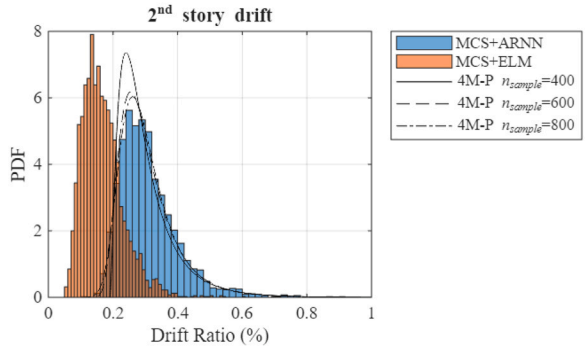

(b) 2nd Story Drift PDF.

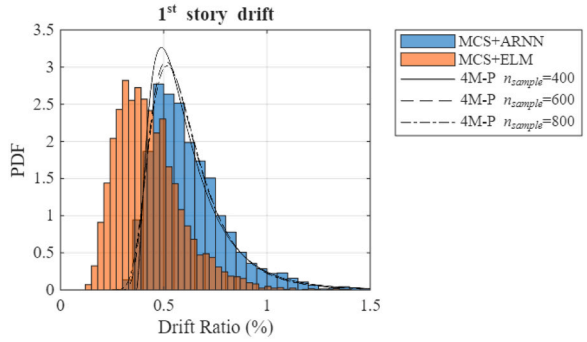

(c) 1st Story Drift PDF.

Fig. 10. Comparison of PDF generated using MCS and 4M-P.

Higher discrepancies in P_f at lower probability levels are likely due to the limited MCS sample size, which restricts the accuracy of rare event estimation.

For the linearized method, the MCS + ELM results show an underprediction compared to those obtained using ARNN. This observation is consistent with findings in the literature [44], which report that equivalent linearized models for base isolators tend to underestimate structural displacement. As also illustrated in Fig. 10, the discrepancy between ARNN and ELM increases with story height, with ELM consistently underpredicting the drift response. Table 8 presents the P_f values computed from MCS + ELM under different drift thresholds, showing significantly lower P_f estimates compared to the ARNN-based assessment in Table 7 due to the underprediction of ELM.

All three assessment methods 4M-P, MCS + ARNN, and MCS + ELM consistently indicate that the lower story governs the critical failure limit state, exhibiting the largest drift ratio, which is nearly twice that of the upper stories, as shown in Fig. 10. The second and third stories display relatively similar drift ratios. A similar trend is also observed in the ELM-based evaluation. In terms of failure probability (P_f), Table 7 shows that the base story has a P_f value approximately an order of magnitude higher than that of the upper stories.

Overall, the procedure outlined in Section 3 and validated in Section 4 demonstrates that the proposed framework can assess the failure probability of base-isolated steel structures under ground motion and structural parameter uncertainties with accuracy comparable to NTHA, but at a fraction of the computational cost.

5. Conclusion

This study proposes a framework to assess the failure probability of a three-story base-isolated structure by incorporating uncertainties from both ground motion and structural parameters. Unlike most reliability studies, which typically focus on uncertainties in either structural or seismic parameters, the present framework integrates both sources of uncertainty while maintaining NTHA-level accuracy. To achieve computational efficiency, an Artificial Neural Network in the form of an ARNN is developed to predict displacement time history responses. In contrast to many AI-based approaches that predict only peak structural indicators, the constructed ARNN generates complete displacement time histories with acceptable accuracy, as demonstrated in Section 4.1. The integration of this surrogate model with a 4M-P enables efficient assessment of system failure probability through the construction of a surrogate Pearson distribution.

The main findings of this study are summarized as follows:

Table 8
Computed P_f Using MCS + ELM approach.

Drift Threshold	ELM + MCS		
	Top Story	2nd Story	1st Story
P_f ($\delta > 0.50$ %)	0	0	0
P_f ($\delta > 0.75$ %)	2.50×10^{-3}	0	0
P_f (δ>1.00 %)	4.02×10^{-1}	6.29×10^{-2}	8.57×10^{-3}

Table 7
Computed P_f and error between 4M-P method and MCS.

Drift Threshold	4M-P n_{sample}	Top Story			2nd Story			1st Story		
		4M-P Method (ε)		MCS	4M-P Method (ε)		MCS	4M-P Method (ε)		MCS
P_f ($\delta > 0.50$ %)	400	5.21×10^{-2}	16.7	4.46×10^{-2}	4.24×10^{-2}	13.0	3.75×10^{-2}	7.08×10^{-1}	0.8	7.14×10^{-1}
	600	5.25×10^{-2}	17.6		4.28×10^{-2}	14.0		7.24×10^{-1}	1.4	
	800	4.51×10^{-2}	0.9		3.89×10^{-2}	3.8		7.23×10^{-1}	1.3	
P_f ($\delta > 0.75$ %)	400	2.14×10^{-3}	40.2	3.57×10^{-2}	5.09×10^{-3}	78.2	2.86×10^{-3}	1.83×10^{-1}	6.1	1.95×10^{-1}
	600	2.77×10^{-3}	22.5		4.38×10^{-3}	53.2		1.80×10^{-1}	7.9	
	800	2.13×10^{-3}	40.4		3.55×10^{-3}	24.4		1.76×10^{-1}	9.5	
P_f ($\delta > 1.00$ %)	400	7.65×10^{-5}	-	0	8.44×10^{-4}	18.2	7.14×10^{-4}	4.85×10^{-2}	0.1	4.86×10^{-2}
	600	1.63×10^{-4}	-		6.59×10^{-4}	7.8		4.21×10^{-2}	13.2	
	800	1.21×10^{-4}	-		4.87×10^{-4}	31.8		3.92×10^{-2}	19.4	

1. The ARNN model demonstrates high efficiency in terms of required training data. For the three-story steel base-isolated structure examined in this study, only about 125 NTHA simulations generated using Kanai–Tajimi ground motions with variations in structural parameters are needed for effective training.
2. Validation using 30 independent test cases not included in the training dataset shows strong agreement with SAP2000 NTHA results. The ARNN predictions achieve MAPE values of 3–7 %, with correlation coefficients exceeding 0.98. The selected displacement time histories further confirm that the ARNN successfully captures record-to-record ground-motion variability as well as changes in key structural parameters such as mass and stiffness.
3. The proposed ARNN reduces the computational demand drastically, requiring approximately 2 s per prediction compared to $\sim$ 20 min per NTHA run. The study also demonstrates that the 4M-P method, using only 800 samples, successfully reproduces the drift-ratio probability distribution obtained from MCS + ARNN. The failure probabilities estimated by 4M-P show relative errors below 10 % for cases with $P_f > 0.2$; larger deviations for small P_f are attributed to the limited MCS sample size.
4. Although the ELM provides a simplified linear approach with reduced computational effort compared to full NTHA, it consistently underpredicts structural displacement and drift ratios, resulting in unconservative reliability estimates. In terms of computation time, the ELM-based LTHA requires $\sim$ 8 s still higher than the ARNN prediction time for single simulation.

Overall, the proposed framework enables seismic reliability assessment of base-isolated structures with accuracy comparable to NTHA while explicitly incorporating uncertainties from both ground motion and structural parameters. Although errors remain due to ARNN prediction accuracy and surrogate distribution construction, these are within acceptable engineering limits (*MAPE* 4–7 % for ARNN predictions and $<$ 10 % error for 4M-P reliability estimation). The study highlights the potential of combining AI-based surrogate models with advanced probabilistic methods to achieve computationally efficient yet accurate reliability assessments for practical structural design and evaluation.

6. Limitation and future direction

The present study aims to introduce an efficient framework for structural reliability assessment by integrating ARNN with NTHA simulation data and the 4M-P reliability assessment method. However, several limitations remain, as outlined below:

1. The developed ARNN model uses four hidden layers with 50 nodes each, without further hyperparameter tuning, including the window data sizes N_{wr} and N_{wg}. Due to the high computational cost of the ARNN training phase, optimization of these parameters was not performed.
2. The ARNN training 4M-P reliability assessment relied on artificial ground motions generated using the Kanai–Tajimi model. Although these motions are reasonably realistic, they cannot fully capture certain characteristics of real earthquakes, such as near-fault effects or complex out-of-phase behavior.
3. The study is limited to a low-complexity, three-story base-isolated structure, which may not represent more complex structural systems.
4. While the 4M-P reliability method provides efficient and reasonably accurate PDF estimation, it has limitations regarding input moments, as discussed by Zhao et al. [20].

These limitations suggest several potential research directions:

1. Optimization of ARNN hyperparameters to improve predictive accuracy.
2. Use of more advanced or real ground-motion datasets, including near-fault records.
3. Application of ARNN to more complex structures, such as bridges, systems with additional damping devices, or structures considering soil–structure interaction.
4. Integration with alternative or complementary reliability assessment methods.

CRediT authorship contribution statement

Han Aylie: Writing – review & editing, Validation, Supervision, Software, Resources, Funding acquisition. **Marc Ottele:** Writing – review & editing, Supervision. **John Thedy:** Writing – original draft, Validation, Methodology, Formal analysis, Conceptualization. **Iswandi Imran:** Writing – review & editing, Validation, Conceptualization. **Bobby Rio Indriyantho:** Writing – review & editing. **Mochammad Qomaruddin:** Writing – review & editing.

Declaration of Generative AI and AI-assisted technologies in the writing process

During the preparation of this work the author(s) used ChatGPT in order to for language refinement. After using this tool/service, the author(s) reviewed and edited the content as needed and take(s) full responsibility for the content of the publication.

Declaration of Competing Interest

The authors declare that they have no known competing financial interests or personal relationships that could have appeared to influence the work reported in this paper.

Acknowledgments

This study was supported by the Research World Class University (RWCU) program from the Institute for Research and Community Service (LPPM) Universitas Diponegoro through the Decreed no. 222-756/UN7.D2/PP/IV/2025. The support is gratefully acknowledged.

References

[1] V GT, K RM. Properties of steel for use in LRFD. J Struct Div 1978;104:1459–68. https://doi.org/10.1061/JSDEAG.0004988.
[2] Ellingwood BR. LRFD: implementing structural reliability in professional practice. Eng Struct 2000;22:106–15. https://doi.org/10.1016/S0141-0296(98)00099-6.
[3] Rubinstein RY, Kroese DP. Simulation and the Monte Carlo method. Wiley; 2011. ⟨https://books.google.com.tw/books?id=yWcvT80gQK4C⟩.
[4] Olsson A, Sandberg G, Dahlblom O. On Latin hypercube sampling for structural reliability analysis. Struct Saf 2003;25:47–68. https://doi.org/10.1016/S0167-4730(02)00039-5.
[5] Melchers RE. Importance sampling in structural systems. Struct Saf 1989;6:3–10. https://doi.org/10.1016/0167-4730(89)90003-9.
[6] Thedy J, Liao K-W. Multisphere-based importance sampling for structural reliability. Struct Saf 2021;91:102099. https://doi.org/10.1016/j.strusafe.2021.102099.
[7] Au SK, Ching J, Beck JL. Application of subset simulation methods to reliability benchmark problems. Struct Saf 2007;29:183–93. https://doi.org/10.1016/j.strusafe.2006.07.008.
[8] Papaioannou I, Papadimitriou C, Straub D. Sequential importance sampling for structural reliability analysis. Struct Saf 2016;62:66–75. https://doi.org/10.1016/j.strusafe.2016.06.002.
[9] E MR. Radial importance sampling for structural reliability. J Eng Mech 1990;116:189–203. https://doi.org/10.1061/(ASCE)0733-9399(1990)116:1(189).
[10] Grooteman F. Adaptive radial-based importance sampling method for structural reliability. Struct Saf 2008;30:533–42. https://doi.org/10.1016/j.strusafe.2007.10.002.
[11] Roussouly N, Petitjean F, Salaun M. A new adaptive response surface method for reliability analysis. Prob Eng Mech 2013;32:103–15. https://doi.org/10.1016/j.probengmech.2012.10.001.
[12] Gayton N, Bourinet JM, Lemaire M. CQ2RS: a new statistical approach to the response surface method for reliability analysis. Struct Saf 2003;25:99–121. https://doi.org/10.1016/S0167-4730(02)00045-0.

[13] Ghosh J, Padgett JE, Dueñas-Osorio L. Surrogate modeling and failure surface visualization for efficient seismic vulnerability assessment of highway bridges. Prob Eng Mech 2013;34:189–99. https://doi.org/10.1016/j.probengmech.2013.09.003.
[14] Echard B, Gayton N, Lemaire M. AK-MCS: an active learning reliability method combining Kriging and Monte Carlo Simulation. Struct Saf 2011;33:145–54. https://doi.org/10.1016/j.strusafe.2011.01.002.
[15] Roy A, Chakraborty S. Support vector machine in structural reliability analysis: a review. Reliab Eng Syst Saf 2023;233:109126. https://doi.org/10.1016/j.ress.2023.109126.
[16] Thedy J, Liao K-W. Reliability-based structural optimization using adaptive neural network multisphere importance sampling. Struct Multidiscip Optim 2023;66:119. https://doi.org/10.1007/s00158-023-03571-3.
[17] Fauriat W, Gayton N. AK-SYS: An adaptation of the AK-MCS method for system reliability. Reliab Eng Syst Saf 2014;123:137–44. https://doi.org/10.1016/j.ress.2013.10.010.
[18] M HA, C LN. Exact and invariant second-moment code format. J Eng Mech Div 1974;100:111–21. https://doi.org/10.1061/JMCEA3.0001848.
[19] Zhao-Hui L, Dong-Zhu H, Yan-Gang Z. Second-order fourth-moment method for structural reliability. J Eng Mech 2017;143:6016010. https://doi.org/10.1061/(ASCE)EM.1943-7889.0001199.
[20] Zhao Y-G, Lu Z-H. Applicable range of the fourth-moment method for structural reliability. J Asian Archit Build Eng 2007;6:151–8. https://doi.org/10.3130/jaabe.6.151.
[21] Dolinski K. First-order second-moment approximation in reliability of structural systems: critical review and alternative approach. Struct Saf 1982;1:211–31. https://doi.org/10.1016/0167-4730(82)90027-3.
[22] Anerican Society of Civil Engineers. Minimum design loads and associated criteria for buildings and other structures. Am Soc Civ Eng 2017. https://doi.org/10.1061/9780784414248.bm.
[23] De Risi R, Goda K, Tesfamariam S. Multi-dimensional damage measure for seismic reliability analysis. Struct Saf 2019;78:1–11. https://doi.org/10.1016/j.strusafe.2018.12.002.
[24] Wang J, Xu J, Hu X. BIM-based seismic reliability analysis and visualization for RC structures. J Build Eng 2025;106:112475. https://doi.org/10.1016/j.jobe.2025.112475.
[25] Vazirizade SM, Nozhati S, Zadeh MA. Seismic reliability assessment of structures using artificial neural network. J Build Eng 2017;11:230–5. https://doi.org/10.1016/j.jobe.2017.04.001.
[26] Shen J, Pan J, Ding G, Cao L, Zhong Z, Chen J. Seismic reliability analysis of frame structure subjected to sequential ground motions using probability density evolution method. J Build Eng 2025;112:113667. https://doi.org/10.1016/j.jobe.2025.113667.
[27] Fereshtehnejad E, Banazadeh M, Shafieezadeh A. System reliability-based seismic collapse assessment of steel moment frames using incremental dynamic analysis and Bayesian probability network. Eng Struct 2016;118:274–86. https://doi.org/10.1016/j.engstruct.2016.03.057.
[28] Rofooei FR, Mobarake A, Ahmadi G. Generation of artificial earthquake records with a nonstationary Kanai–Tajimi model. Eng Struct 2001;23:827–37. https://doi.org/10.1016/S0141-0296(00)00093-6.
[29] Kim T, Kwon O-S, Song J. Deep learning based seismic response prediction of hysteretic systems having degradation and pinching. Earthq Eng Struct Dyn 2023;52:2384–406. https://doi.org/10.1002/eqe.3796.
[30] Kim T, Kwon O-S, Song J. Deep learning-based response spectrum analysis method for bridges subjected to bi-directional ground motions. Earthq Eng Struct Dyn 2025;54:2031–43. https://doi.org/10.1002/eqe.4345.
[31] Kim T, Kwon O-S, Song J. Response prediction of nonlinear hysteretic systems by deep neural networks. Neural Netw 2019;111:1–10. https://doi.org/10.1016/j.neunet.2018.12.005.
[32] Angarita C, Montes C, Arroyo O. Pushover-ML: a machine learning approach to predict a trilinear approximation of pushover curves for low-rise reinforced concrete frame buildings. SoftwareX 2025;30:102122. https://doi.org/10.1016/j.softx.2025.102122.
[33] Mahmoudi H, Bitaraf M, Salkhordeh M, Soroushian S. A rapid machine learning-based damage detection algorithm for identifying the extent of damage in concrete shear-wall buildings. Structures 2023;47:482–99. https://doi.org/10.1016/j.istruc.2022.11.041.
[34] Hooshyar H, Ahmadi HR, Bayat M, Hosseinzadeh E, Mahdavi N, Najafi MH. New method for damage detection in steel beam using time-frequency functions and machine learning. Structures 2025;78:109236. https://doi.org/10.1016/j.istruc.2025.109236.
[35] Egatama HF, Indriyantho BR, Han AL, Nouchi E, Wijayaningsih ES, Gan BS. Quantification of shaking-based criteria for evaluating aseismic performance of house and building. Iran J Sci Technol Trans Civ Eng 2024;48:4333–47. https://doi.org/10.1007/s40996-024-01411-y.
[36] Ning C, Xie Y, Sun L. LSTM, WaveNet, and 2D CNN for nonlinear time history prediction of seismic responses. Eng Struct 2023;286:116083. https://doi.org/10.1016/j.engstruct.2023.116083.
[37] Jia J, Gong M, Zuo Z, Liu B. Real-time structural seismic time history response prediction based on physics-informed deep learning. J Build Eng 2025;108:112932. https://doi.org/10.1016/j.jobe.2025.112932.
[38] Shen Yongxi, Ma Gao, Hwang Hyeon-Jong, Kim Dae-Jin, Zhang Zhenhao. Prediction of seismic response of building structures using a CNN-LSTM-ATT network with transfer learning. Adv Struct Eng 2025:13694332251340730. https://doi.org/10.1177/13694332251340730.
[39] Cheynet E. Earthquake simulation and fitting. 2020. https://doi.org/10.5281/zenodo.3774069.
[40] Shrimali MK, Bharti SD, Dumne SM. Seismic response analysis of coupled building involving MR damper and elastomeric base isolation. Ain Shams Eng J 2015;6:457–70. https://doi.org/10.1016/j.asej.2014.12.007.
[41] S N, K SM, D BS, K DT. Collapse of damaged steel building frames because of earthquakes. J Perform Constr Facil 2018;32:4017128. https://doi.org/10.1061/(ASCE)CF.1943-5509.0001125.
[42] Shivachandra VA, Dayal BS, Kumar SM, Kanti DT. Optimum coefficient of friction in FPS for base isolation of building frames. Pract Period Struct Des Constr 2022;27:4022042. https://doi.org/10.1061/(ASCE)SC.1943-5576.0000722.
[43] Liao K-W, Wang Y-I, Chen C-C. Probabilistic seismic performance evaluation of steel moment frame using high-strength and high-ductility steel. Constr Build Mater 2018;184:151–64. https://doi.org/10.1016/j.conbuildmat.2018.06.194.
[44] Dicleli M, Buddaram S. Comprehensive evaluation of equivalent linear analysis method for seismic-isolated structures represented by sdof systems. Eng Struct 2007;29:1653–63. https://doi.org/10.1016/j.engstruct.2006.09.013.